Acta Crystallographica Section F
Structural Biology and Crystallization Communications
ISSN 1744-3091

Crystallization and preliminary X-ray diffraction analysis of rat autotaxin

Jacqueline E. Day,[a] Troii Hall,[a]‡ Lyle E. Pegg,[a] Timothy E. Benson,[a] Jens Hausmann[b] and Satwik Kamtekar[a]*§

[a]Pfizer Global Research and Development, St Louis Laboratories, 700 Chesterfield Parkway West, Chesterfield, MO 63017, USA, and [b]Division of Biochemistry, The Netherlands Cancer Institute, Plesmanlaan 121, 1066 CX Amsterdam, The Netherlands

‡ Current address: Leinco Technologies, 359 Consort Drive, St Louis, MO 63011, USA.
§ Current address: Pacific Biosciences, 1505 Adams Drive, Menlo Park, CA 94025, USA.

Correspondence e-mail: satwik.kamtekar@gmail.com

Received 27 June 2010
Accepted 29 July 2010

Rat autotaxin has been cloned, expressed, purified to homogeneity and crystallized *via* hanging-drop vapour diffusion using PEG 3350 as precipitant and ammonium iodide and sodium thiocyanate as salts. The crystals diffracted to a maximum resolution of 2.05 Å and belonged to space group *P*1, with unit-cell parameters a = 53.8, b = 63.3, c = 70.5 Å, α = 98.8, β = 106.2, γ = 99.8°. Preliminary X-ray diffraction analysis indicated the presence of one molecule per asymmetric unit, with a solvent content of 47%.

1. Introduction

Autotaxin (ATX), which is also known as (ecto)nucleotide pyrophosphatase/phosphodiesterase 2 (ectoNPP2), functions as an extracellular phosphodiesterase/pyrophosphatase that mediates the conversion of lysophosphatidylcholine (LPC) to lysophosphatidic acid (LPA) (Umezu-Goto *et al.*, 2002). Mature ATX consists of two somatomedin domains, an NPP domain and a MORPHO (modulator of oligodendrocyte remodelling and focal adhesion organization) domain (Yuelling & Fuss, 2008). It is approximately 98 kDa in size. It is a glycoprotein and it has been shown that only one of the four ATX glycosylation sites is required for functional activity (Jansen *et al.*, 2007).

ATX plays a role in a wide range of functions *in vivo*, from the conversion of LPC to LPA and the differentiation of myelinating oligodendrocytes (Yuelling & Fuss, 2008) to lymphocyte entry into lymphoid organs (Kanda *et al.*, 2008). ATX has been proposed to be an important central nervous system, gastrointestinal, oncology, inflammation and immunology target (Khurana *et al.*, 2008; Inoue *et al.*, 2008; Prestwich *et al.*, 2008; Kehlen *et al.*, 2001). Medicinal chemistry efforts have identified several classes of ATX inhibitors (Prestwich *et al.*, 2008; van Meeteren *et al.*, 2008); Cui *et al.*, 2007; Saunders *et al.*, 2008; Ferry *et al.*, 2008; Parrill *et al.*, 2007). As there are no publicly disclosed structures of closely related enzymes, an ATX structure would deepen our understanding of its basic biological roles as well as accelerate the design and development of promising drug candidates.

The laboratory of Anastassis Perrakis at the Netherlands Cancer Institute (NKI) have designed a mutant rat ATX (rATX) construct that yielded a complete data set to 2.4 Å resolution (Hausmann *et al.*, 2010). In the process of reproducing and optimizing crystallization with this construct, we found a new crystallization condition that resulted in larger, more mechanically robust and less radiation-sensitive crystals. Here, we describe the results obtained for the optimized crystallization of rATX and its X-ray diffraction data to 2.05 Å resolution.

2. Experimental procedure

2.1. Expression and purification of rat autotaxin

The rATX mutant cell line (Hausmann *et al.*, 2010) was thawed into a T75 flask, incubated at 5% CO_2 and 310 K and expanded into T175 flasks upon confluency. The growth medium was DMEM supplemented with 10% FBS, penicillin/streptomycin, 2 m*M* glutamine

Table 1
Data-collection statistics for rATX crystals.

Values in parentheses are for the highest resolution shell.

Crystal data	
No. of crystals	1
Beamline	APS 23-ID-D
Detector	MAR Mosaic 300
Total rotation/rotation per frame (°)	460/1
Space group	*P*1
Unit-cell parameters (Å, °)	a = 53.8, b = 63.3, c = 70.5, α = 98.8, β = 106.2, γ = 99.8
Data collection	
Wavelength (Å)	1.28299
Mosaicity (°)	0.4
Resolution (Å)	20.0–2.05 (2.12–2.05)
Total No. of reflections†	511856
No. of unique data	52153
Multiplicity	4.8 (3.0)
Data completeness (%)	96.8 (93.9)
Average $I/\sigma(I)$	13.9 (2.49)
$R_{\rm merge}$‡	0.097 (0.378)
Molecules per asymmetric unit	1
Matthews coefficient (Å^3 Da^{-1})	2.3
Solvent content (%)	47

† This value includes measurements of partial reflections. ‡ $R_{\rm merge} = \sum_{hkl}\sum_i |I_i(hkl) - \langle I(hkl)\rangle| / \sum_{hkl}\sum_i I_i(hkl)$.

(final concentration) and 100 mg l^{-1} hygromycin (Invitrogen). Two confluent T175 flasks were used to seed each roller bottle (Greiner Bio One) containing 800 ml growth medium. The roller bottles were maintained at 5% CO_2 and 310 K. When the cells began to reach confluency, the medium was harvested semi-weekly and replaced with the same growth medium containing 5% FBS. The roller bottles were maintained until the cells began to fall off the surface.

rATX was purified using an adaptation of the procedure described by Hausmann *et al.* (2010). All purification procedures were performed at 278 K unless otherwise noted. 50 m*M* Tris–HCl pH 8.0 and 300 m*M* NaCl were added to 1 l HEK media. 5 ml Ni^{2+}–NTA Superflow resin was added and the protein was allowed to batch bind overnight. The resin slurry was poured into an XK26 column and the flowthrough was collected. 20 column volumes of buffer were used to wash the resin, followed by another four column volumes of buffer containing 20 m*M* imidazole. The protein was eluted using four column volumes of buffer containing 150 m*M* imidazole. The eluate was diluted threefold with 50 m*M* Tris pH 8.0 to lower the conductivity to below 7 mS and the protein was batch bound for 1 h to an optional 5 ml Q-Sepharose FF resin. The resin slurry was poured into an XK26 column and washed with a step gradient using three column volumes of 50 m*M* Tris pH 8.0 containing 75 m*M* NaCl followed by three column volumes of buffer containing 150 m*M* NaCl. Samples containing autotaxin with a purity greater than 85% as determined by SDS–PAGE were concentrated to less than 5 ml using an Amicon-10 and loaded onto a Superdex 200 (16/60) column equilibrated with 50 m*M* Tris pH 8.0, 300 m*M* NaCl. Fractions containing autotaxin with a purity greater than 95% were pooled, concentrated to approximately 10 mg ml^{-1} and subsequently diluted to 5 mg ml^{-1} with 50 m*M* Tris pH 8.0. The purified and concentrated autotaxin was then aliquoted, flash-frozen on dry ice and stored at 193 K. Protein concentrations were determined from the $A_{280\,\rm nm}$ using an extinction coefficient of 1.0 AU ml mg^{-1}.

2.2. Crystallization

Initial crystallization screening was carried out at 295 K using Art Robbins CrystalMation Intelli-Plate 96-3 sitting-drop vapor-diffusion trays (catalog No. HR3-118 from Hampton Research) by mixing 300 nl protein solution with 300 nl precipitant solution and equilibrating against 85 µl well solution. A Mosquito robot (TTP LabTech) was used to set up multiple crystallization screens using rATX at a concentration of 3.5–5.0 mg ml^{-1} in 50 m*M* Tris pH 8.0 (277 K) and 150 m*M* NaCl. The original crystallization condition (condition No. 12 from the PEG/Ion crystallization screen; Hampton Research) was further optimized by the addition of 0.24–0.34 *M* sodium thiocyanate to yield a final well volume of 500 µl in an SBS footprint 24-well hanging-drop vapor-diffusion tray. These results were not reproducible with alternate sources of ammonium iodide other than the well solution purchased from Hampton Research. The best crystals were obtained using 3 µl of a spin-filtered protein solution and 1.5 µl well solution. A simple substitution of seed stock (prepared by crushing a single crystal in 50 µl precipitant solution) for well solution in crystallization drops dramatically increased the number of crystals formed.

2.3. X-ray data collection and processing

All crystals were soaked for 2 s in a cryoprotective solution consisting of crystallization solution supplemented with 15% glycerol and an additional 15% PEG 3350 prior to flash-freezing to 100 K by plunging the crystals into liquid nitrogen. A native data set was collected at 50 eV above the zinc edge on beamline 23-ID-D at APS, which is equipped with a MAR Mosaic 300 detector. A complete data set was obtained using several wedges of data from a single crystal with multiple translations to alleviate the effects of radiation damage. The data were processed using *DENZO* and *SCALEPACK* from the *HKL*-2000 package (Otwinowski & Minor, 1997); statistics are summarized in Table 1.

3. Results

rATX crystals grew in a multitude of PEG-based conditions. However, the best crystals grew from PEG/Ion Screen (Hampton Research) condition No. 12 (20% PEG 3350, 0.2 *M* ammonium iodide) supplemented with 0.3 *M* sodium thiocyanate. The most reproducible single crystals grew from drops set up with seed stock. The crystals reached maximum dimensions of 0.15 × 0.05 × 0.05 mm in two weeks (Fig. 1). A complete X-ray data set was collected to 2.05 Å resolution from a single native rATX crystal, with some frames showing spots to 1.9 Å resolution (Fig. 2). Specific volume calculations based on the molecular weight of rATX and the unit-cell parameters indicated the presence of a single molecule in the

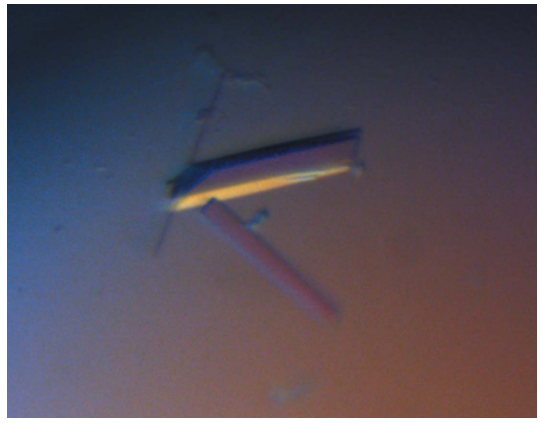

Figure 1
Native rATX crystals obtained using 20% PEG 3350, 0.2 *M* ammonuim iodide solution supplemented with 0.3 *M* sodium thiocyanate. The approximate dimensions of the crystals are 0.15 × 0.05 × 0.05 mm.

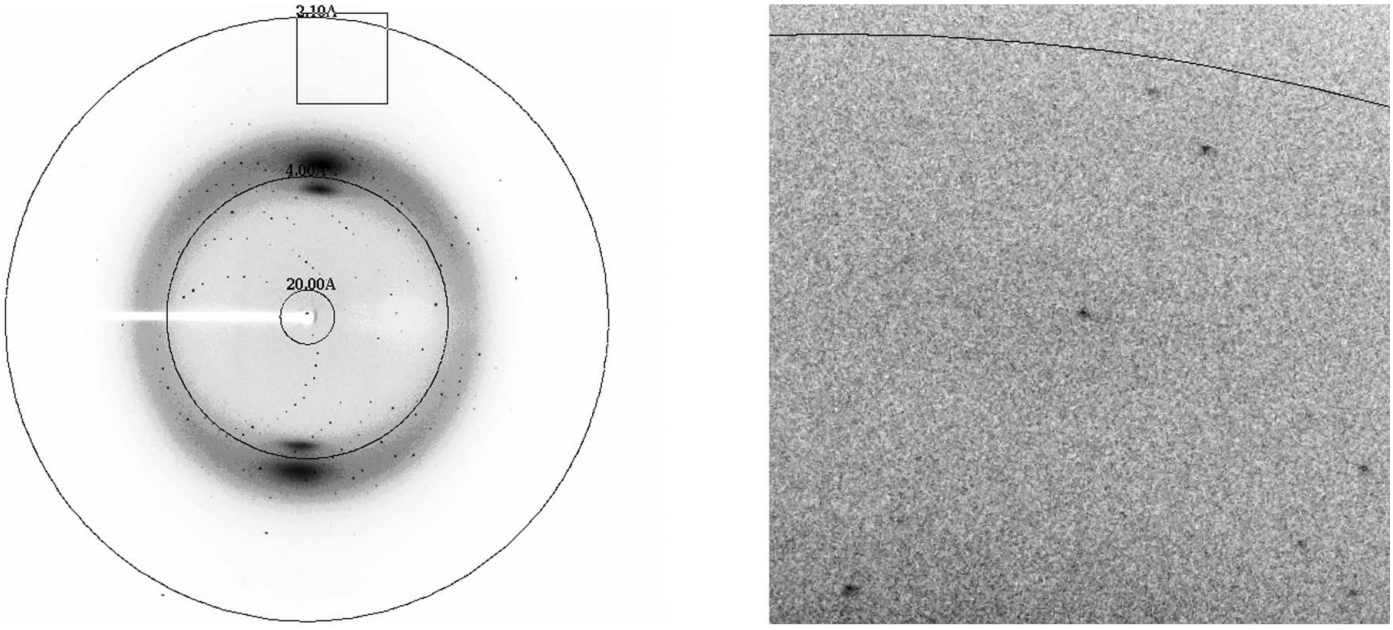

Figure 2
(*a*) X-ray diffraction pattern of an rATX crystal (oscillation range 1.0°); (*b*) an enlargement (with a different brightness and contrast) showing the highest resolution area (the resolution ring is at 2.1 Å).

asymmetric unit, with 47% solvent content and a Matthews coefficient of 2.3 Å^3 Da^{-1} (Matthews, 1968). Structure determination was initiated using the Xac nucleotide pyrophosphatase/phosphodiesterase structure (PDB code 2gsn; Zalatan *et al.*, 2006) as the initial model; this enzyme shares 30% sequence identity with the NPP domain of rATX. The program *Phaser* (McCoy *et al.*, 2007) yielded a rotation-function *Z* score of 14.4 using reflections to 3.0 Å resolution. The high resolution and the presence of a single molecule in the asymmetric unit make this an appropriate crystal form for structure determination and refinement.

The authors wish to thank the staff of the 23-ID-D (GM/CA-CAT), 21-ID-D (LS-CAT) and 24-ID-E (NE-CAT) beamlines at the APS for support during synchrotron data collection. Use of the Advanced Photon Source at Argonne National Laboratory was supported by the US Department of Energy, Office of Science, Office of Basic Energy Sciences under Contract No. DE-AC02-06CH11357.

References

Cui, P., McCalmont, W., Tomsig, J., Lynch, K. & Macdonald, T. (2007). *Bioorg. Med. Chem.* **16**, 2212–2225.
Ferry, G., Moulharat, N., Pradère, J., Desos, P., Try, A., Genton, A., Giganti, A., Beucher-Gaudin, M., Lonchampt, M., Bertrand, M., Saulnier-Blache, J., Tucker, G., Cordi, A. & Boutin, J. (2008). *J. Pharmacol. Exp. Ther.* **327**, 809–819.
Hausmann, J., Christodoulou, E., Kasiem, M., De Marco, V., van Meeteren, L. A., Moolenaar, W. H., Axford, A., Owen, R. L., Evans, G. & Perrakis, A. (2010). *Acta Cryst.* F**66**, 1130–1135.
Inoue, M., Ma, L., Aoki, J., Chun, J. & Ueda, H. (2008). *Mol. Pain*, **4**, 4–6.
Jansen, S., Callewaert, N., Dewerte, I., Andries, M., Ceulemans, H. & Bollen, M. (2007). *J. Biol. Chem.* **282**, 11084–11091.
Kanda, H., Newton, R., Klein, R., Morita, Y., Gunn, M. & Rosen, S. (2008). *Nature Immunol.* **4**, 415–423.
Kehlen, A., Lauterbach, R., Santos, A. N., Thiele, K., Kabisch, U., Weber, E., Riemann, D. & Langner, J. (2001). *Clin. Exp. Immunol.* **123**, 147–154.
Khurana, S., Tomar, A., George, S., Wang, Y., Siddiqui, M., Guo, H., Tigyi, G. & Mathew, S. (2008). *Exp. Cell Res.* **3**, 530–542.
Matthews, B. W. (1968). *J. Mol. Biol.* **33**, 491–497.
McCoy, A. J., Grosse-Kunstleve, R. W., Adams, P. D., Winn, M. D., Storoni, L. C. & Read, R. J. (2007). *J. Appl. Cryst.* **40**, 658–674.
Otwinowski, Z. & Minor, W. (1997). *Methods Enzymol.* **276**, 307–326.
Parrill, A., Echols, U., Nguyen, T., Pham, T., Hoeglund, A. & Baker, D. (2007). *Bioorg. Med. Chem.* **16**, 1784–1795.
Prestwich, G. D., Gajewiak, J., Zhang, H., Xu, X., Yang, G. & Serban, M. (2008). *Biochim. Biophys. Acta*, **9**, 588–594.
Saunders, L., Ouellette, A., Bandle, R., Chang, W., Zhou, H., Misra, R., De La Cruz, E. & Braddock, D. (2008). *Mol. Cancer Ther.* **7**, 3352–3362.
Umezu-Goto, M., Kishi, Y., Taira, A., Hama, K., Dohmae, N., Takio, K., Yamori, T., Mills, G., Inoue, K., Aoki, J. & Arai, H. (2002). *J. Cell Biol.* **158**, 227–233.
Van Meeteren, L., Brinkmann, V., Saulnier-Blache, J., Lynh, K. & Moolenaar, W. (2008). *Cancer Lett.* **266**, 203–208.
Yuelling, L. M. & Fuss, B. (2008). *Biochim. Biophys. Acta*, **9**, 525–530.
Zalatan, J. G., Fenn, T. D., Brunger, A. T. & Herschlag, D. (2006). *Biochemistry*, **45**, 9788–9803.